Accepted Manuscript

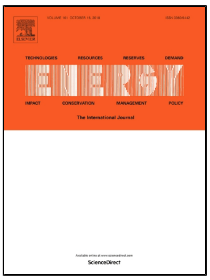

Heat transmission over long pipes: new model for fast and accurate district heating simulations

A. Dénarié, M. Aprile, M. Motta

PII:	S0360-5442(18)31958-3
DOI:	10.1016/j.energy.2018.09.186
Reference:	EGY 13880
To appear in:	*Energy*
Received Date:	29 January 2018
Accepted Date:	27 September 2018

Please cite this article as: A. Dénarié, M. Aprile, M. Motta, Heat transmission over long pipes: new model for fast and accurate district heating simulations, *Energy* (2018), doi: 10.1016/j.energy.2018.09.186

This is a PDF file of an unedited manuscript that has been accepted for publication. As a service to our customers we are providing this early version of the manuscript. The manuscript will undergo copyediting, typesetting, and review of the resulting proof before it is published in its final form. Please note that during the production process errors may be discovered which could affect the content, and all legal disclaimers that apply to the journal pertain.

ACCEPTED MANUSCRIPT

Title

Heat transmission over long pipes: new model for fast and accurate district heating simulations

Authors

A. Dénarié ([1]), M. Aprile, M. Motta

Department of Energy, Politecnico di Milano, 20156 Milano, Italy

Highlights

- Heat-transmission model based on the method of characteristics
- Inclusion of the thermal capacity effect related to the turbulent boundary layer
- Calculation 10^3 times faster than the finite-volume method at the same level of accuracy
- Very good agreement with experimental data

[1] Corresponding author. Tel.: +39 02 2399 3850; fax: +39 02 2399 3868.

E-mail address: alice.denarie@polimi.it (A. Dénarié).

ACCEPTED MANUSCRIPT

Abstract

This paper presents a new numerical approach to model the heat transmission over long pipes, such as those encountered in district heating networks. The model is suitable for fast and accurate simulation of complex network dynamics. For fast calculation, the model is based on the method of characteristics. For high accuracy, the model splits the water thermal capacity between the turbulent core and the boundary layer. Compared with the finite-volume method and the node method, the proposed model shows accurate results at a lower computational expense and without introducing artificial smoothing of temperature waves. The model is validated by monitoring data of pronounced temperature transients in real pipes at low and high Reynolds numbers. The results confirm the need to properly model the thermal capacity of water, because at a low Reynolds number, the boundary-layer thickness is considerable, and the temperature difference between the water core and the pipe wall is not negligible.

Keywords

District heating, heat transmission in pipes, dynamic model, turbulent flow, transient temperature simulation.

ACCEPTED MANUSCRIPT

ACCEPTED MANUSCRIPT

Summary

ACCEPTED MANUSCRIPT

ACCEPTED MANUSCRIPT

Abbreviations

CHP Combined Heat and Power

Cu Courant number

DH District Heating

FVM Finite Volume Method

Nu Nusselt number

ODE Ordinary Differential Equation

PDE Partial Differential Equation

Re Reynolds number

Nomenclature

A area, m^2

c_p specific heat, J kg^{-1} K^{-1}

h linear heat transfer coefficient, W m^{-1} K^{-1}

L pipe length, m

$\dot{m}$ mass flow rate, kg s^{-1}

$\dot{Q}$ heat transfer rate, W

R pipe radius, m

r distance from the inner pipe wall, m

s parameter of characteristics method

T temperature, °C

t time, s

v fluid velocity, m s^{-1}

ACCEPTED MANUSCRIPT

x pipe section length, m

Greek symbols

δ water turbulent boundary layer thickness, m

θ temperature, advection problem solution, °C

ρ density, kg m^{-3}

Subscripts

B equivalent boundary layer (water boundary layer and steel pipe)

b water boundary layer

c turbulent core

ext external environment

i pipe number

in inlet section of the pipe

ins insulation

j timestep number

k pipe segment number

lin linear

out outlet section of the pipe

s steel pipe

t temperature

w water

ACCEPTED MANUSCRIPT

ACCEPTED MANUSCRIPT

1 INTRODUCTION

District heating (DH) has demonstrated great potential for increasing the efficiency of urban heat-distribution systems in Europe, by using and efficiently distributing heat that would otherwise be wasted [1, 2]. However, traditional European combined heat and power (CHP)-based DH systems risk losing their attractiveness in terms of energy efficiency, CO_2 emissions savings, and financial profitability. The current energy framework introduces new challenges for DH [3]: the increase of renewables in power production and the parallel decrease of electricity consumption [4] have reduced the use of CHP plants, while the majority of DH systems usually recover their rejected heat. The search for waste heat to be recovered and the exploitation of local renewable energy sources have become concrete alternatives: DH utilities exhibit an increasing amount of waste heat and renewable energy distributed along the network.

The needs and energy loads of DH consumers are evolving as well. In the new paradigm of distributed generation, consumers will increasingly become prosumers who can actively interact with the DH network [5]. In addition, the amount of low-energy buildings will increase among DH consumers. In light of these new challenges, low-temperature networks and subnetworks appear to be promising and economical solutions [6–8].

The temperatures profiles for these types of networks are, on average, lower and, over short timescales, exhibit greater fluctuation than those characterising traditional DH systems. The variety of generation systems and the variety of user demand profiles increase the network complexity; thus, the network should be analysed carefully, considering the system dynamics.

The interactions of these elements during both the design and operational phases, can be predicted using detailed dynamic simulation models. The DH system involves three main dynamic elements: energy production, distribution network, and consumers. Their dynamics heavily affect the control and management of the entire system. For traditional systems with centralised production and similar customers, simplified modelling approaches can be used without affecting the quality of the results [9]. In contrast, new-generation DH systems involve a variety of energy sources, and the customers create distributed points of interest along the network. Heat losses, pressure drops, and considerable time delays strongly affect the temperatures and pressures at distant points of the network, which become substantially different from those of the central plant. Thus, analysis requires a robust and flexible simulation model of the entire network that is able to simulate distributed energy sources.

1.1 PREVIOUS WORKS

The most commonly used mathematical model for thermohydraulic networks is the pseudo-dynamic model [10], in which the hydraulic problem is considered to be steady-state while the thermal problem is treated as a transient phenomenon. This because of the difference in the propagation speed between the pressure waves and water. The hydraulic problem is usually solved using the Hardy Cross method and the Newton–Raphson method [11], which involve iteration in the case of meshed networks. In [12], a new method for solving the steady-state hydraulics of complex networks was presented as more efficient and easier than the Hardy Cross method.

The simulation of the temperature propagation and its dynamics, which is the primary interest of this work, can be grouped into two main modelling categories [13].

- Black-box models, in which only the inputs and outputs of the system are considered. They can be statistical, regressive, artificial neural network [14], or transfer-function models.
- Physical models, in which the physical aspects of the system are modelled explicitly.

A third branch of research in modelling networks has the main objective of reducing the network complexity by building a simpler equivalent network model to perform real-time optimisation. The topology of the network is thus simplified in an equivalent model with a lower number of pipes. With this kind of approach, the computational costs decrease, but the link with the topology is lost; thus, this method is mostly suitable for centralised systems. Two main reduction approaches are found in the literature: the Danish one and the German one [9].

Early works regarding physical models were performed in Denmark, beginning with the element method, which is a finite-difference method that solves energy-balance equations. This was followed by the node method approach, which is commonly used in Denmark, whereby the pipe temperatures are calculated using the time history of the inflow temperature and the mass flowrate. This method was elaborated by Benonysson [10]. Benonysson reports that the accuracy of the element method cannot compensate for its long calculation time, which affects the usability of this method. Another drawback of the element method is the occurrence of artificial diffusion if discretisation in time and space produces a Courant number other than 1. The strength of the node method is that, via the plug-flow approach, it only calculates the temperature at the outlet of each pipe, according to the propagation time of the inlet temperature decreased by thermal losses. Thus, the computational efforts are significantly reduced. A rigorous theoretical analysis of these two methods is provided in [13]. Further work on finite-difference modelling can be found in [15, 16], where a two-dimensional model comprising pre-insulated twin pipes is compared with other models and experimental measurements.

ACCEPTED MANUSCRIPT

The node method has shown good performance for object-oriented modelling. In [17], Giraud et al. present a Modelica library conceived to simulate DH networks and solar thermal integration. In [18], Van Der Heijde et al. show a Modelica software implementation of a thermohydraulic model for thermal networks and validate it experimentally. The plug-flow approach is also the basis of pipe model Type 31 in the TRNSYS software library [19]. TRNSYS is a dynamic simulation software used for solar thermal plants and building energy performance.

On the other hand, Gabrielaitiene has provided major contributions through several studies comparing the node method with other modelling approaches [20], using the commercial software TERMIS [21–23] and DH monitoring data [24]. The main outcomes of these comparisons are significant discrepancies between the simulated temperatures and the monitored ones at distant points of the networks that are reached after passing through several bends and connections. The model also reveals insufficient performances in simulating rapid and sharp temperature variations, thus showing an inability to properly model fast dynamics [20].

1.2 MOTIVATION OF STUDY

The need for analysing peripheral points of DH systems has increased in recent years, leading to studies regarding network analysis and simulations of DH with decentralised generation systems [25–28]. In this study, a new modelling approach for heat transmission along the DH network, which is based on the method of characteristics [29], is proposed and compared with existing models. The method of characteristics allows partial differential equations (PDEs) to be solved by reducing them to an equivalent system of ordinary differential equations (ODEs).

A good compromise between the accuracy and rapidity of the model must be reached to perform detailed energy simulation of complex networks.

Finite-element methods based on discretisation have shown good accuracy but high computational costs. The node method is faster but is inaccurate for distant points of the network with sharp temperature variations. According to the node method analysis in [20], the discrepancies between the measured temperatures and simulations are larger for

- long pipelines;
- turbulent flows at relatively low Reynolds numbers.

The most important heat capacity in DH modelling is that of water. The overall conclusion from previous studies is that to improve simulation results, a detailed model of the turbulent flow characteristics must be employed [20]. Accordingly, in the present study, an improved plug-flow model for simulating long pipelines

was developed. The model is suitable for DH system modelling, as it allows fast and accurate simulations of the thermal and hydraulic behaviour of the water flow in long pipes.

2 MATHEMATICAL MODEL

The model is constructed in MATLAB®. The equations constituting the overall model are presented here. In the second step, the model is enhanced by separating the turbulent fluid core and the boundary layer. The transient model is based on the following assumptions:

- The water is considered as an incompressible and homogenous fluid;
- Thermal diffusion in the axial direction is neglected;
- There is no thermal stratification in the pipe section;
- There is axial symmetry in the temperature and velocity profiles inside the section;
- The material properties have constant values.

2.1 ONE-CAPACITY FLUID MODEL

The energy-balance equations describing heat transmission allow the pipe and water temperatures to be calculated as a function of the axial length x and time t:

$$\begin{cases} \rho_w A_w c_{p,w} \frac{\partial T_w}{\partial t} + \dot{m}_w c_{p,w} \frac{\partial T_w}{\partial x} + h_{sw}(T_w - T_s) = 0 \\ \rho_s A_s c_{p,s} \frac{\partial T_s}{\partial t} + h_{sw}(T_s - T_w) + h_{ins}(T_s - T_{ext}) + \dot{Q}_{lin}^{\leftarrow} = 0 \end{cases}, \tag{2.1}$$

where $A_w = \pi R_w^2$ is the internal cross section of the pipe [m^2], $A_s = \pi(R_s^2 - R_w^2)$ is the cross section of the steel pipe, T_{ext} is the temperature of the environment surrounding the pipe (ground), and $\dot{Q}_{lin}^{\leftarrow}$ is a generic linear source of heat [W/m]. The linear insulation heat-transfer coefficients for insulation and steel [30] are calculated as $h_{ins} = \frac{2\pi k_{ins}}{ln(R_{ins}/R_s)}$ and $h_s = \frac{2\pi k_s}{ln(R_s/R_w)}$, respectively. For the inner surface of the steel pipe, the water–steel linear insulation heat-transfer coefficient is calculated as $h_{sw} = 1/(\frac{1}{h_w} + \frac{1}{h_s})$. The heat transfer among the three elements involved—water, steel, and insulation—can be represented by the thermal resistor–capacitor network (Figure 2.1). Here, the temperature distribution in the section is approximated using two lumped capacitance nodes for the water and pipe, as well as an external temperature node.

ACCEPTED MANUSCRIPT

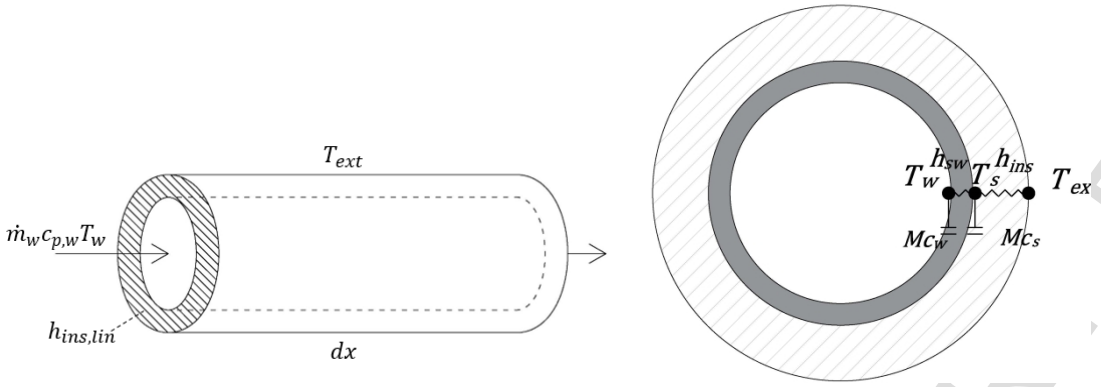

Figure 2.1 Longitudinal and transversal pipe section—the transversal capacity nodes considered are the water (w) and steel pipe (s)

By neglecting the source of heat, for simplification, the system (2.1) can be rewritten as

$$\begin{aligned} &\frac{\partial T_w}{\partial t} + v\frac{\partial T_w}{\partial x} + \frac{h_{sw}}{\rho_w A_w c_{p,w}}\left(T_w - T_s\right) = 0 \\ &\frac{\partial T_s}{\partial t} + \frac{h_{sw}}{\rho_s A_s c_{p,s}}\left(T_s - T_w\right) + \frac{h_{ins}}{\rho_s A_s c_{p,s}}\left(T_s - T_{ext}\right) = 0 \end{aligned}, \tag{2.2}$$

where $v = \dot{m}/(\rho_w A_w)$ is the mean fluid velocity in the section.

The problem (2.2) is a system of inhomogeneous hyperbolic conservation laws [29]. The mathematical approach that can be used to solve them is the splitting approach [29], which consists of splitting—for a certain time step Δt—the system (2.2) into a homogenous PDE advection problem (2.3) and an ODE source problem (2.4) to be solved in succession.

$$\begin{cases} \dfrac{\partial \theta_w}{\partial t} + v\dfrac{\partial \theta_w}{\partial x} = 0 \\ \theta_w(x,t_0) = T_{w0}(x) \end{cases} \tag{2.3}$$

Here, θ_w is the temperature for the homogenous advection PDE (2.3). For each coordinate $\bar{x}$, the solution at $t_0 + \Delta t$ is the solution of the source problem (2.4), in which the initial condition at time t_0 is set equal to the solution of the advection problem $\tilde{\theta}_w$ at time $t_0 + \Delta t$:

$$\begin{bmatrix} \dfrac{dT_w}{dt} \\ \dfrac{dT_s}{dt} \end{bmatrix} = \begin{bmatrix} -\dfrac{h_{sw}}{\rho_w A_w c_{p,w}} & \dfrac{h_{sw}}{\rho_w A_w c_{p,w}} \\ \dfrac{h_{sw}}{\rho_s A_s c_{p,s}} & -\dfrac{h_{sw} + h_{ins}}{\rho_s A_s c_{p,s}} \end{bmatrix} \begin{bmatrix} T_w \\ T_s \end{bmatrix} + \begin{bmatrix} 0 \\ \dfrac{h_{ins}}{\rho_s A_s c_{p,s}} T_{ext} \end{bmatrix} \tag{2.4}$$

$$\begin{matrix} T_w(\overline{x},t_0) = \tilde{\theta}_w(\overline{x},t_0 + \Delta t) \\ T_s(\overline{x},t_0) = T_{s0}(\overline{x}) \end{matrix} .$$

2.1.1 Advection problem: one-equation model

The homogenous part of the system (2.2) belongs to the class of homogenous hyperbolic conservation laws [29] that can be solved via the method of characteristics [29, 31], which states the equivalence of the original problem (2.3) to the solution of the auxiliary system (2.5):

$$\begin{cases} \dfrac{dt}{ds} = 1 \\ \dfrac{dx}{ds} = v \\ \dfrac{d\theta_w}{ds} = 0 \end{cases} \tag{2.5}$$

$$\theta_w(0) = T_w(x_0) .$$

The auxiliary system is composed of the characteristic equations, in which x and t are parametrised by s. The solution of this system stipulates that the temperature profile θ_w is constant along the trajectories given by the two solutions $t(x_0,s)$ and $x(x_0,s)$ of (2.6):

$$\begin{cases} t(x_0,s) = s + t_0 \\ x(x_0,s) = v\, s + x_0 \\ \theta_w = cost \end{cases} . \tag{2.6}$$

When s is eliminated, the characteristic curve—in this case, a line—is $x = v\,\Delta t + x_0$ (with $\Delta t = t - t_0 = s$). Along this curve, the constancy of the temperature profile is valid. With θ_w being constant, the initial value is chosen so that

$$\theta_w = T_w(x_0) = T_w(x - v\,\Delta t). \tag{2.7}$$

This formulation yields an easy solution to the advection problem: at a certain time step t_j, the water temperature is $T_w^j(x) = T_w^{j-1}(x - v\,\Delta t)$. This solution can be discretised in space by approximating the initial temperature profile inside the pipe as a step function in x, i.e., by subdividing the water volume in the pipe into a sequence of finite volumes of homogeneous temperature. If $\underline{x}^j$ and $\underline{\theta}_w^j$ are vectors containing the position and temperature at time step j of each volume, the temperature propagation at time step $j+1$ can be computed according to the characteristic lines by adding a new element to the two vectors, which corresponds to the position and temperature of the incoming water volume. The position of the remaining volumes is shifted by $v\,dt$, as shown in Figure 2.2.

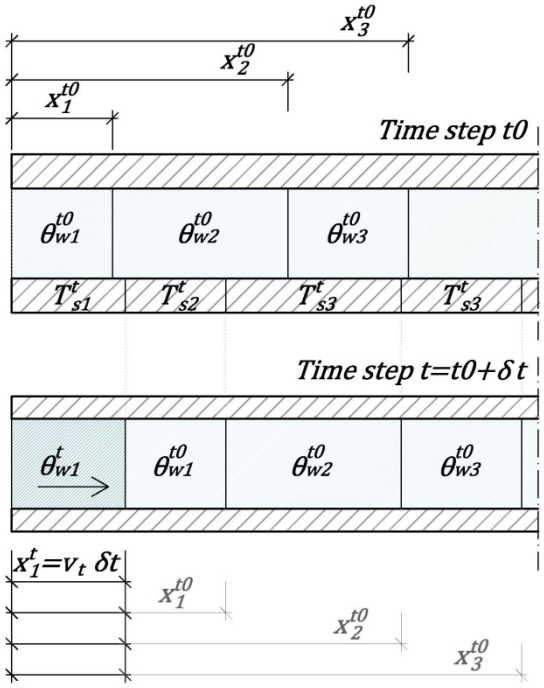

Figure 2.2 Temperature propagation according to characteristic lines

2.1.2 Source problem: two-equation model

Once the advection problem is solved, the effects of the heat losses and thermal capacities can be accounted for by solving the source problem. For the generic discrete water volume k, the matrix form of system (2.6), $\frac{d\underline{T}_k}{dt} = [A]_k \underline{T}_k + \underline{b}_k$, can be analytically solved as follows:

$$\begin{cases} T_{w,k} = c_{1k} V_{1k} e^{\lambda_{1k}\Delta t_k} + c_{2k} W_{1k} e^{\lambda_{2k}\Delta t_k} + T_{ext} \\ T_{s,k} = c_{1k} V_{2k} e^{\lambda_{1k}\Delta t_k} + c_{2k} W_{2k} e^{\lambda_{2}k\Delta t_k} + T_{ext} \end{cases}, \tag{2.8}$$

where λ_{1k},λ_{2k} and $\underline{V}_k$,$\underline{W}_k$ are the eigenvalues and eigenvectors of matrix $[A]_k$, and c_{1k},c_{2k} are constants calculated by applying the initial conditions. Importantly, the water temperature profile inside the pipe is a step function, and the elements of vector $\underline{x}^j$ are determined by the flowrate at every simulation time step. The steel temperature is discretised with the same spatial discretisation so that $\underline{T}_s$ has the same size as $\underline{T}_w$ and $\underline{x}$. Every element $T_{s,k}$ at every timestep j is updated as the average value of the temperatures of the pipe in the sections crossed by water in the time step. The transport time Δt_k of volume k travelling through a pipe of length L_{pipe} is calculated as follows.

$$\Delta t_k = \min\left(\Delta t, \frac{L_{pipe} - x_k}{v}\right) \tag{2.9}$$

In some cases, $\Delta t_k < \Delta t$, which means that during the simulation time step Δt, a portion of the water volume has exited the pipe. Consequently, the same superposition of the source term problem must be applied again for the adjoining pipes. In-depth calculation of the outlet temperature across the junction of the pipes is presented in the following subsection.

2.1.3 Outlet temperature and junctions of pipes

Owing to the vectorial representation of the step function, the proposed model can trace the temperature profile and flow path inside the pipes, as shown in Figure 2.3, along with the water volumes flowing out of the pipes.

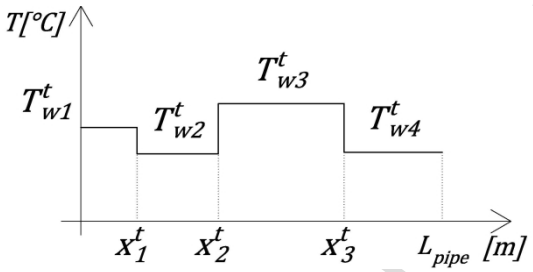

Figure 2.3 Qualitative representation of temperature step function profile, $\underline{x}$ and $\underline{T}_w$

In the case of junctions, the temperature of the water leaving the pipe and entering the adjacent one is a vector, rather than a single value T_{out} as for typical pipe models. The proposed approach traces the temperature profile for the water volume leaving the pipe: $\underline{x}_{out}$ and $\underline{T}_{w_{out}}$. $\underline{x}_{out}$ is determined as

$$\underline{x}_{out} = \max(0, \underline{x} - L_{pipe}), \tag{2.10}$$

and the elements of $\underline{T}_{w_{out}}$ are the temperature steps corresponding to these positions. As shown in the exemplary case of Figure 2.4, new water volumes move from one pipe to the next in the flow direction of vt.

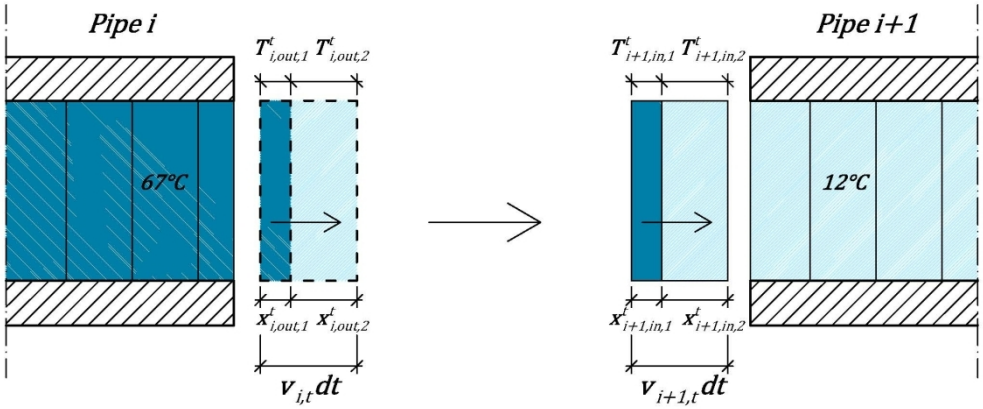

Figure 2.4 Details of the outlet water temperature profile; initial temperature: 12 °C, step input at 67 °C

In the case of a connection between two pipes, i and $i+1$, with different sections, the mass and energy balances are applied:

$$\begin{cases} \underline{x}_{i+1,in} = \underline{x}_{i,out} \dfrac{v_{i+1}}{v_i} \\ \underline{T}_{w,i+1,in} = \underline{T}_{w,i,out} \end{cases}. \tag{2.11}$$

In the case of two water flows mixing in a single pipe, the energy and mass conservation equations are applied to the three temperature profiles involved. Because the two flows coming from the two meeting pipes have different spatial discretisations $\underline{x}_{1,out}$ and $\underline{x}_{2,out}$, a new common discretisation is formulated: $\underline{x}_3 = \cup\left(\underline{x}_{3,1}, \underline{x}_{3,2}\right)$, where $\underline{x}_{3,1}$ and $\underline{x}_{3,2}$ are calculated from $\underline{x}_{1,out}$ and $\underline{x}_{2,out}$, respectively, according to (2.11). Each $T_{w3,k}$ of $\underline{x}_3$ is calculated as follows.

$$\begin{cases} \dot{m}_1 + \dot{m}_2 = \dot{m}_3 \\ \dot{m}_1 T_{w1,k} + \dot{m}_2 T_{w2,k} = \dot{m}_3 T_{w3,k} \end{cases} \tag{2.12}$$

Figure 2.5 illustrates this approach in an exemplary case.

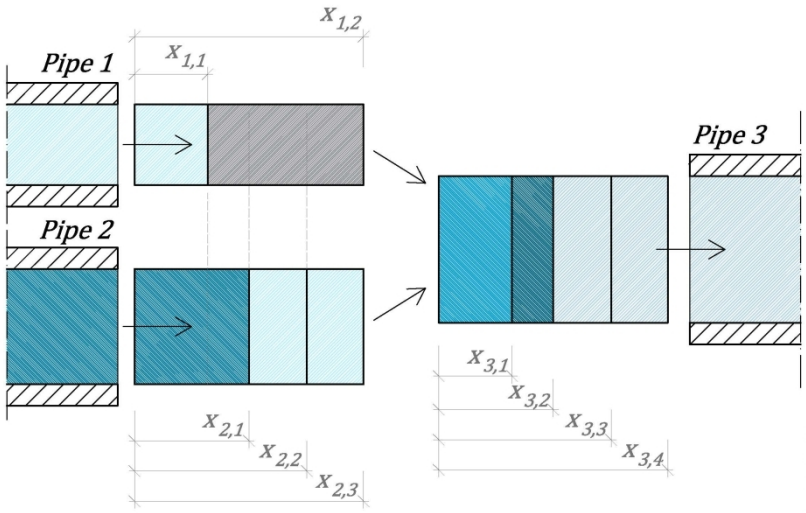

Figure 2.5 Mixing in new approach model

This guarantees that the number of joints of the pipes and the discretisation do not influence the final results. On the other hand, this mixing calculation increases the number of steps in the temperature profile. To limit this phenomenon, a maximum number of allowed steps is defined, and the two adjacent segments with the closest temperatures are combined into an equivalent one, maintaining the internal energy conservation. The model aspects related to the temperature profile of the outlet water volume are particularly important because, as shown in Chapter 3, they are the main difference from the existing Lagrangian modelling approaches and have been identified as the major cause of inaccurate modelling of distant network points.

2.2 TWO-CAPACITY FLUID MODEL

The presented model is extended to a two-capacity fluid model to include the turbulent flow characteristics. With a low Reynolds number, the non-uniformity of the water section is not neglected. The boundary layer is the region of the pipe section in which the entire gradient of the temperature and velocity is concentrated. Its thickness δ is small with respect to the entire section, but at relatively low velocity and in a large pipe section, it can represent a significant water mass that has different behaviour from the turbulent core.

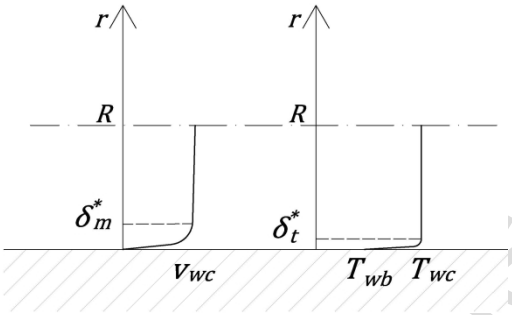

Figure 2.6 Qualitative velocity and temperature distribution in the turbulent flow in a half-section of the pipe

Figure 2.6 illustrates the qualitative flow and temperature distribution in a half-section of the pipe with turbulent flow. The momentum (or velocity) and temperature viscous boundary layers—δ_m^* and δ_t^*, respectively—are the regions in which the velocity and temperature profiles are influenced by the pipe wall and can be approximated as linear [32]. To include the boundary-layer characteristics, the model described by (2.2) is modified by splitting the node representing water in the turbulent core node and the node representing the boundary layer (see Figure 2.7):

$$\begin{aligned}
&\frac{\partial T_{wc}}{\partial t} + v_{wc}\frac{\partial T_{wc}}{\partial x} + \frac{h_w}{\rho_w A_{wc} c_{p,w}}\left(T_{wc} - T_{wb}\right) = 0 \\
&\frac{\partial T_{wb}}{\partial t} + v_{wb}\frac{\partial T_{wb}}{\partial x} + \frac{h_w}{\rho_w A_{wb} c_{p,w}}\left(T_{wb} - T_{wc}\right) + \frac{h_s}{\rho_w A_{wb} c_{p,w}}\left(T_{wb} - T_s\right) = 0 \\
&\frac{\partial T_s}{\partial t} + \frac{h_s}{\rho_s A_s c_{p,s}}\left(T_s - T_{wb}\right) + \frac{h_{ins}}{\rho_s A_s c_{p,s}}\left(T_s - T_{ext}\right) = 0\,,
\end{aligned} \tag{2.13}$$

where $A_{wc} = \pi(R_w - \delta_m^*)^2$ is the turbulent core section area, and $A_{wb} = \pi(R_w^2 - \delta_m^{*2})$ is the boundary-layer area.

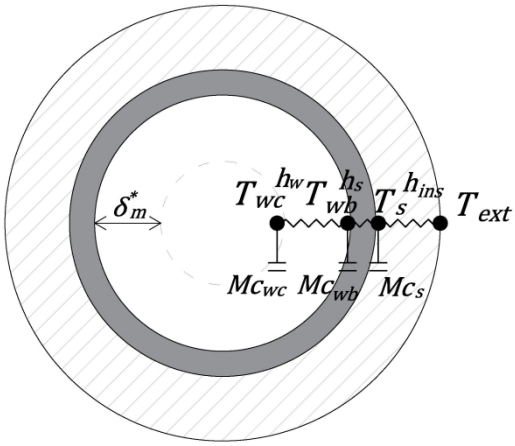

Figure 2.7 Turbulent flow model: water section split in turbulent core and viscous sublayer

The convective heat-transfer coefficient of water flowing in the pipe, h_w, is calculated as follows:

$$h_w = Nu\frac{k_w}{D}\pi D, \tag{2.14}$$

where Nu can be calculated according to the Gnielinski formulation in the validity range of $3 \times 10^3 < Re < 5 \times 10^6$. The boundary-layer thickness is calculated as follows [33].

$$\delta_t^* = \frac{k_w}{h_w^{cv}} \tag{2.15}$$

$$\delta_m^* = \delta_t^* \cdot Pr^{1/3} \tag{2.16}$$

The velocity profile and temperature profile in the section for the turbulent pipe can be approximated as follows [34]:

$$\frac{v_w(r)}{v_w^{max}} = \left(1 - \frac{r}{R}\right)^{1/7} \qquad \text{With } v_w^{max} = \frac{5}{4} v_{wc}\,, \tag{2.17}$$

where v_{wc} is the average core section velocity. The water velocity at $r = \delta_m^*$ can be determined using (2.17), by linearising the gradient in the boundary layer:

$$v_{wb} = \left[\left(1 - \frac{\delta_m^*}{R}\right)^{1/7}\right]\frac{v_w^{max}}{2}\,. \tag{2.18}$$

System (2.13) can be solved using the previously presented approach. Considering that $v_{wc} \gg v_{wb}$, the system can be simplified by merging the water boundary layer and the steel pipe nodes into one single stationary node

with temperature T_B. This allows the system to be reduced to two equations: one for the moving water turbulent core and one for the stationary boundary (including the water boundary layer, steel pipe, and insulation). The source problem of the turbulent flow model becomes

$$\begin{bmatrix} \frac{dT_{wc}}{dt} \\ \frac{dT_B}{dt} \end{bmatrix} = \begin{bmatrix} -\frac{h_B}{\rho_w A_{wc} c_{p,w}} & \frac{h_B}{\rho_w A_{wc} c_{p,w}} \\ \frac{h_B}{C_B} & -\frac{h_B + h_{ins}}{C_B} \end{bmatrix} \begin{bmatrix} T_{wc} \\ T_B \end{bmatrix} + \begin{bmatrix} 0 \\ \frac{h_{ins}}{C_B} T_{ext} \end{bmatrix} \tag{2.19}$$

$$\begin{matrix} T_{wc}(x,0) = \theta_{wc}(x,t) \\ T_B(x,0) = \theta_B(x,t) \end{matrix} ,$$

where $h_B = 1/(\frac{1}{h_w} + \frac{1}{h_s})$ and $C_B = \rho_w A_{wb} c_{p,w} + \rho_s A_s c_{p,s}$.

3 MODEL RESULTS

The model is compared with the most commonly used and validated modelling approaches: the finite-volume method (FVM) and the node method (the one-capacity fluid version). The purpose is to highlight their differences from a numerical standpoint. The two-capacity fluid model is then validated by experimental data.

3.1 COMPARISON WITH OTHER MODELS

The reference DH pipe DN 300, whose characteristics are taken from [20], is used to compare the results for the different models, first in the single-equation form (neglecting the steel-pipe capacity) and then with two equations (considering the steel-pipe capacity). The flow rate of the test pipe is 2.7 m^3/h, which is a typical summer load flowrate.

3.1.1 One-equation model: advection problem

The outlet-temperature step response is compared between the FVM and the newly developed one-equation model in Figure 3.1. Considering the flow velocity, it takes 3.4 h for the water front to reach the outlet section of the pipe. Consequently, the new model shows the exact propagation solution, while the FVM needs intense discretisation to increase the accuracy. The simulation time step for the new model is 0.25 h, whereas the FVM simulation time step changes according to the spatial discretisation, maintaining Cu = 0.95. Table 3.1 shows the corresponding computational effort for the simulation presented in the graph. The plug-flow approach exhibits higher accuracy and a shorter simulation time (Processor i-5 CPU 2.5 GHz).

ACCEPTED MANUSCRIPT

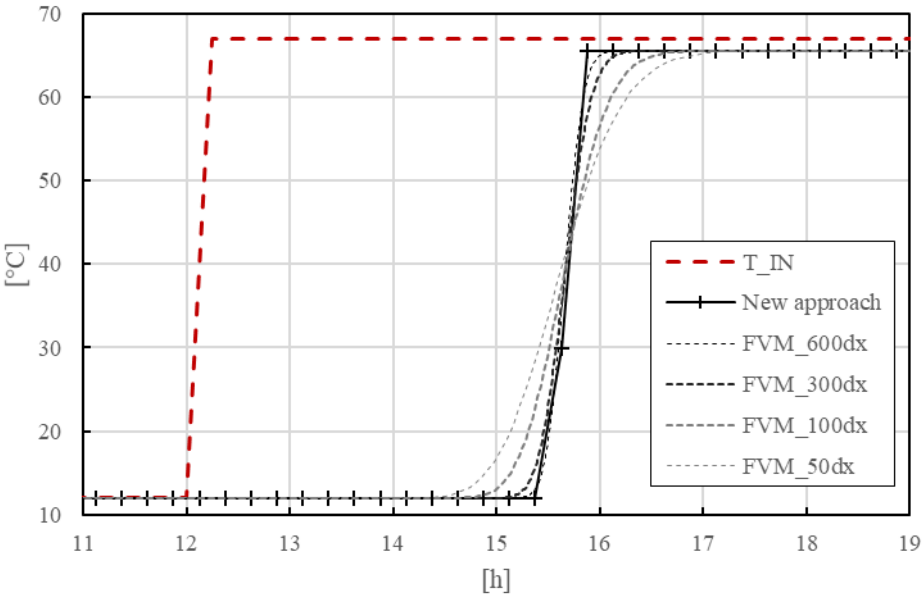

Figure 3.1 Input step response in the adiabatic case

Table 3.1 Simulation time for the reference pipe with the node method and increasing discretisation in the FVM method

	New approach	**FVM method**			
n°dx (discretisation)	**1**	**50**	**100**	**300**	**600**
dx [m]	470	9.4	4.7	1.5	0.7
Simulation time [s]	0.13	2.64	6.08	52.08	453

The same input step is used for comparison with the node method. The node-method outlet temperature calculation [20] is the result of the energy balance applied to the outlet water volume, i.e., the weighted sum of the temperature steps in the outlet water. Depending on the flow velocities and the chosen simulation time step, this mixing can cause temperature smoothing at the pipe ends, as shown in Figure 3.2.

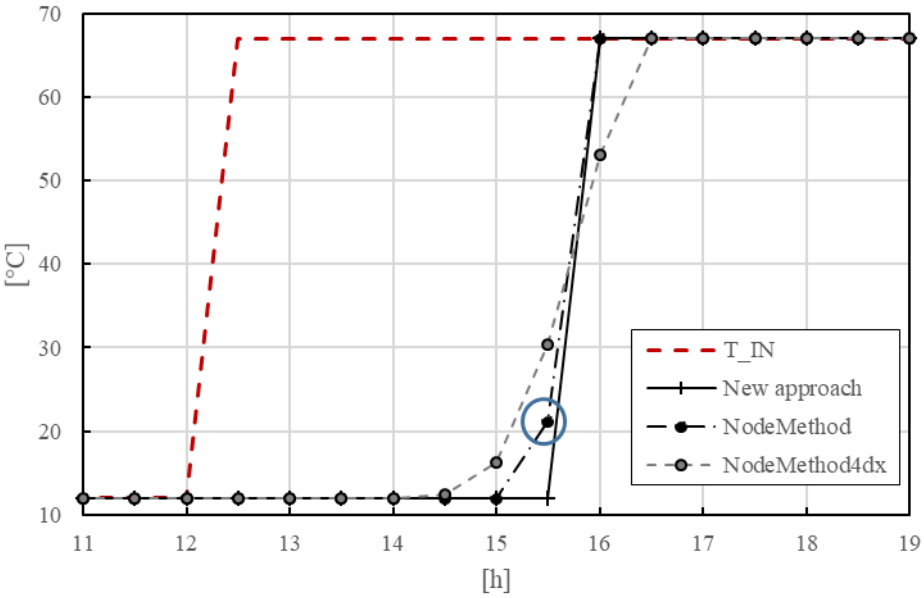

Figure 3.2 Step response for the node method with dt = 0.5 h

Figure 3.2 compares the step input response between the new approach and the node method. With the chosen time step, two water volumes—at 12 and 67 °C—come out of the pipe at the moment the step input reaches the outlet. The mixing approach of the node method creates an intermediate point at 21.22 °C at t = 15.5 h. This mixing effect increases with discretisation: in the figure, the simulation of the pipe divided into four parts has a smoothed result. This smoothing effect is more evident for a larger number of pipes, natural mixing points, and joints of the network. The mixing can be one of the causes of the pronounced discrepancies in the temperatures between the node method and the monitoring data for distant pipelines containing numerous junctions mentioned in [24].

3.1.2 Two-equation model: source problem

Figure 3.3 compares the outlet-temperature step response among the FVM, the node method, and the newly developed two-equation version.

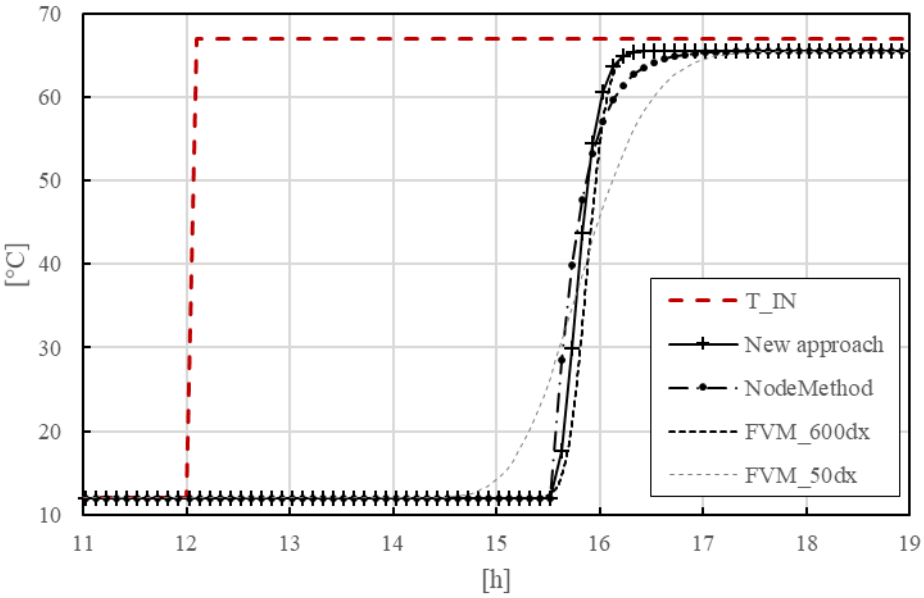

Figure 3.3 Step response for pipe capacity model: FVM (small and large discretisation), node method, and new two-equation model

Again, the new model is significantly faster than the FVM and has high accuracy, shown in Figure 3.3 and Table 3.2.

Table 3.2 Simulation time for the reference pipe: new approach and increasing discretisation for FVM methods in the two-equation model

	New approach	**FVM method**			
n°dx	**1**	**50**	**100**	**300**	**600**
dx [m]	470	9.4	4.7	1.5	0.7
Simulation time [s]	1.14	3.68	10.69	236	2,504.78

The reasons for the difference between the node method and the new approach are related to the mixing phenomenon previously described and to the way the methods deal with the pipe capacity (details in [20]). The node method modifies the solution of the advection problem, θ_w, lumping the entire steel pipe at the outlet node of the pipe and thus neglecting the temperature profile along the pipe. The smoothing effect due to the mixing is still present, as shown in Figure 3.4. Here, the results of sinusoidal inputs to the FVM, the node method, and the new approach are presented, and the mixing effect of the node method is shown by dividing the pipe into ten parts (10 dx).

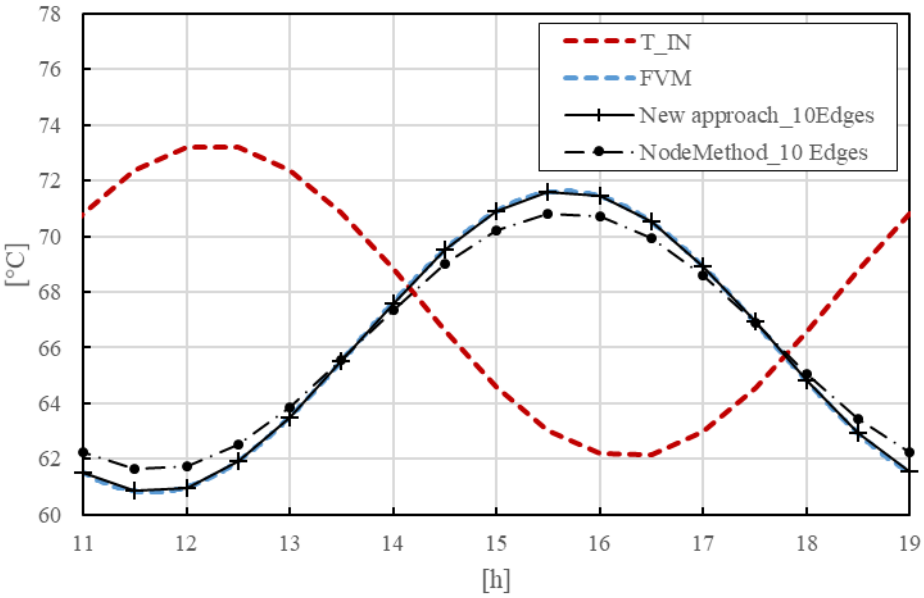

Figure 3.4 Sinusoidal input response in the pipe model considering the steel capacity for the node method, the new approach, and the FVM approach with dt=0.5 h

3.2 EXPERIMENTAL VALIDATION

The validation is performed using two experimental monitoring datasets, as follows.

- Pipe 1: Test rig in the thermodynamics laboratory; pipe length = 39 m, pipe diameter = DN50; monitoring data kindly shared by K. Sartor, University of Liège; further details in [35].
- Pipe 2: single pipe of Vilnius DH taken from [36]; pipe length = 470 m, pipe diameter = DN300.

These two datasets are of interest because the operational conditions are the ones in which the previous models have shown needs for improvement: sharp input temperature variation and low velocity regime.

3.2.1 Experimental validation of Pipe 1

The validation of the new model with the experimental data for Pipe 1 is shown in Figure 3.5. The results of the model are close to the experimental data. With a low Re number, as in the experimental case, v = 0.27 m/s and Re = 3×10^4, and the water convective heat transfer h_w is considerably lower than the usual value for a turbulent flow. The figure shows the different results obtained using the same two-equation approach but with different fluid models: one-capacity and two-capacity.

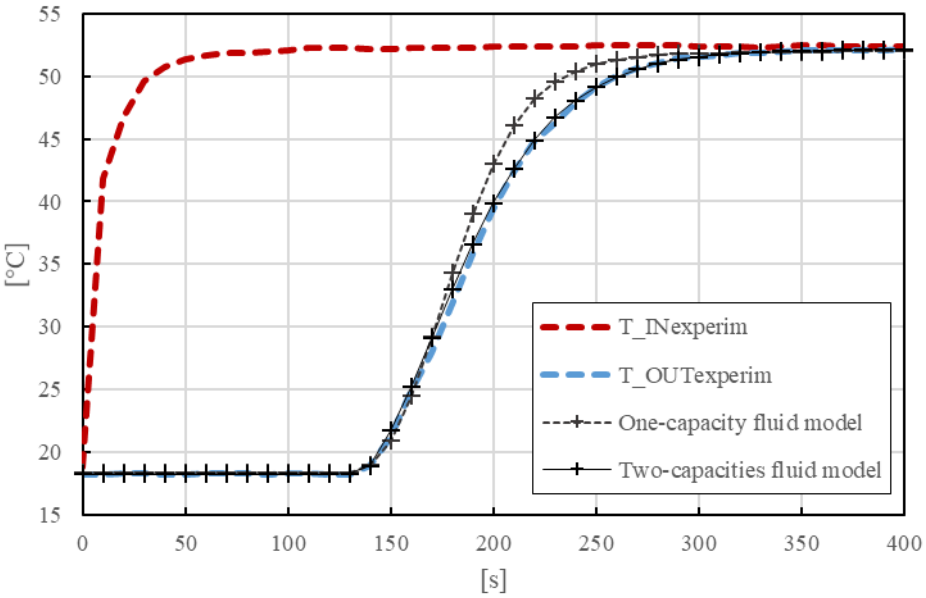

Figure 3.5 Simulation results obtained using the new approach for Pipe 1, with a flow velocity of v = 0.27 m/s

As shown, the two-capacity fluid model results are significantly closer to the real experimental data than the one-capacity model. The relevance of this modelling aspect tends to decrease with the increase of the Reynolds number. The same comparison at a higher velocity (v = 1.05 m/s and Re = 1.17×10^5) is shown in Figure 3.6. Here, the results of the one-capacity and two-capacity models are very similar. A higher fluid velocity yields a smaller thickness of the boundary layer. With a small capacity and high convective heat transfer, the boundary layer has a small effect on the temperature trend.

ACCEPTED MANUSCRIPT

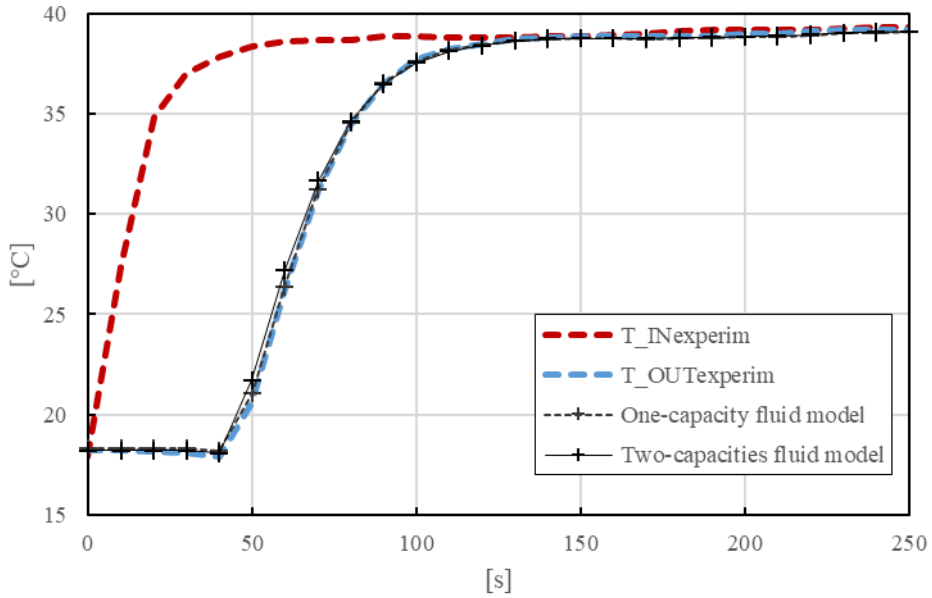

Figure 3.6 Simulation results obtained using the new approach for Pipe 1, with a flow velocity of v = 1.05 m/s

3.2.2 Experimental validation of Pipe 2

The proposed approach is now used to model pipe 2 with the monitoring data of Vilnius DH [36]. This test checks the model validity for a DH pipe under real operating conditions.

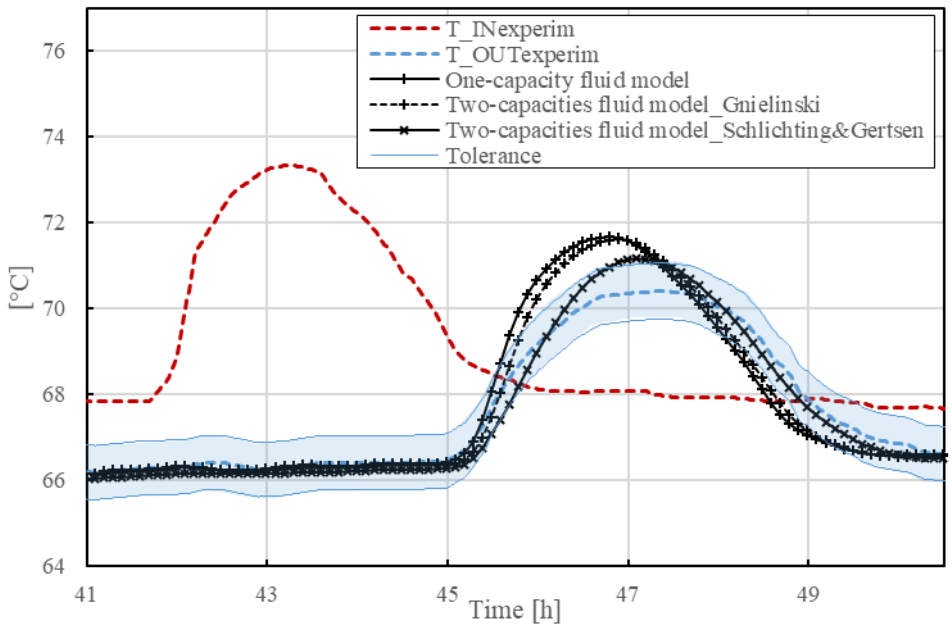

Figure 3.7 Simulation results obtained using the new approach for Pipe 2, with a flow velocity of v = 0.03 m/s

Figure 3.7 shows the results for the one-capacity fluid model and the two-capacity fluid model, where the Gnielinski formulation is used to determine h_w and consequently δ_m^*.

The temperature-profile trend resulting from the simulation with the Gnielinski formulation of h_w appears less smooth than the real profile for the water flowing out of the pipe, with a higher and anticipated temperature peak. The peak temperature is 1.2 °C higher than the monitoring results, and it is observed at the pipe outlet 30 min earlier. It has been verified that with a different distribution of the water capacity between the turbulent core and the boundary layer, greater smoothing occurs. When a larger capacity is assigned to the boundary layer than to the core, the two-capacity fluid model provides a temperature profile closer to the real trend. Importantly, no additional water capacity is added; rather, the capacity is redistributed between nodes, keeping the overall fluid capacity constant.

A different empirical formulation giving a larger value of δ_m^* is consequently applied according to Schlichting and Gersten correlation [37], where the momentum boundary-layer thickness is experimentally approximated as follows.

$$\frac{\delta_m^*}{D} = 122 \frac{\ln Re}{Re\, G} \tag{3.1}$$

Here, G = 1.35 in the flow regime of interest.

The larger value of δ_m^* resulting from (3.1) brings the simulation result closer to the monitoring data, making it almost entirely within the tolerance curves given by the measurement uncertainty [36]: the time of the peak appearance at the pipe outlet corresponds to that in the monitoring result, and the temperature difference between the simulation and the real data is reduced to 0.75 °C.

4 CONCLUSIONS

The proposed method of heat transmission over long pipes shows advantages over other methods, making it a suitable alternative for the simulation of complex DH network dynamics. The improved plug-flow model considers the temperature difference between the fluid core and the viscous sublayer in a turbulent flow, while it reduces the error propagation in long pipes. The mathematical approach used to solve the thermal transmission problem—the splitting approach—yields accurate results with low computational effort.

ACCEPTED MANUSCRIPT

The model results are comparable to those of the high-discretisation FVM, but the proposed model is faster and does not include artificial diffusion. Compared with the node method, it retains the simulation speed, avoiding sharp temperature variation smoothing.

Summarising the main findings, the new approach has

- the same accuracy as the finest-discretisation FVM, while being 10^3 times faster;
- the rapidity of the node method but without the smoothing effect of sharp temperature variations;
- better correspondence to experimental data with respect to the one-capacity fluid model in terms of the time delay and temperature value of peak phenomena—the temperature difference is reduced from 1.2 to 0.75 °C.

Finally, the new model was shown to accurately predict the propagation of temperature waves compared with monitoring data. The inclusion of the water viscous boundary layer in the modelling approach improved the simulation results for low-velocity turbulent flows in DH pipes.

As indicated by its good results, the model can be applied to simulate real operational conditions. Thus, it is suitable for DH system modelling, as it allows fast and accurate simulation of the thermal and hydraulic behaviour of the water flow in long pipes.

Future research will consist of modelling an entire DH network and comparing the simulation results with monitoring data.

Acknowledgements

The authors gratefully acknowledge Kevin Sartor from Thermodynamics Laboratory (B49) of University of Liège (ULg) for sharing experimental data.

ACCEPTED MANUSCRIPT

ACCEPTED MANUSCRIPT

References

[1] S. Werner, Ecoheatcool WP4: Possibilities with more district heating in Europe, 2006. http://www.euroheat.org/Files/Filer/ecoheatcool/documents/Ecoheatcool_WP4_Web.pdf.

[2] U. Persson, S. Werner, District heating in sequential energy supply, Appl. Energy. 95 (2012) 123–131. doi:10.1016/j.apenergy.2012.02.021.

[3] A. Dénarié, M. Calderoni, M. Muscherà, Technical, Financial and Urban Potentials for Solar District Heating in Italy, in: A. Bisello, D. Vettorato, R. Stephens, P. Elisei (Eds.), Smart Sustain. Plan. Cities Reg. Results SSPCR 2015, Springer International Publishing, Cham, 2017: pp. 15–32. doi:10.1007/978-3-319-44899-2_2.

[4] Terna Group, Dati Storici, (2015) retrived from www.terna.it. https://www.terna.it/it-it/sistemaelettrico/statisticheeprevisioni/datistorici.aspx (accessed May 26, 2017).

[5] L. Brange, J. Englund, P. Lauenburg, Prosumers in district heating networks - A Swedish case study, Appl. Energy. 164 (2016) 492–500. doi:10.1016/j.apenergy.2015.12.020.

[6] A. Dalla Rosa, R. Boulter, K. Church, S. Svendsen, District heating (DH) network design and operation toward a system-wide methodology for optimizing renewable energy solutions (SMORES) in Canada: A case study, Energy. 45 (2012) 960–974. doi:10.1016/j.energy.2012.06.062.

[7] H. Lund, S. Werner, R. Wiltshire, S. Svendsen, J.E. Thorsen, F. Hvelplund, B.V. Mathiesen, 4th Generation District Heating (4GDH): Integrating smart thermal grids into future sustainable energy systems, Energy. 68 (2014) 1–11. doi:10.1016/j.energy.2014.02.089.

[8] A.D. Rosa, The Development of a new District Heating Concept Network Design and Optimization for Integrating Energy Conservation and Renewable Energy Use, PhD Thesis, Technical University of Denmark (DTU), Denmark, 2012.

[9] H. V Larsen, B. Bøhm, M. Wigbels, A comparison of aggregated models for simulation and operational optimisation of district heating networks, Energy Convers. Manag. 45 (2004) 1119–1139. doi:10.1016/j.enconman.2003.08.006.

[10] A. Benonysson, Dynamic modelling and operation optimization of district heating systems, PhD Thesis, Technical University of Denmark (DTU), Denmark, 1991.

[11] I. Ben Hassine, U. Eicker, Impact of load structure variation and solar thermal energy integration on an existing district heating network, Appl. Therm. Eng. 50 (2013) 1437–1446.

doi:10.1016/j.applthermaleng.2011.12.037.

[12] V.D. Stevanovic, S. Prica, B. Maslovaric, B. Zivkovic, S. Nikodijevic, Efficient numerical method for district heating system hydraulics, Energy Convers. Manag. 48 (2007) 1536–1543. doi:10.1016/j.enconman.2006.11.018.

[13] H. Pálsson, Methods for planning and operating decentralised combined heat and power plants, PhD Thesis, Riso National Laboratory, Roskilde, Danemark, 2000. http://orbit.dtu.dk/files/51481519/Halldor.PDF.

[14] K. Sartor, D. Thomas, P. Dewallef, A comparative study for simulating heat transport in large district heating networks, in: ECOS 2015 Int. Conf., Pau, France, 2015. http://orbi.ulg.ac.be/request-copy/2268/183406/247807/?step=4&token=7e8b59730f22b74d262334d8d99ae256&id=1 (accessed June 21, 2017).

[15] A. Dalla Rosa, H. Li, S. Svendsen, Method for optimal design of pipes for low-energy district heating, with focus on heat losses, Energy. 36 (2011) 2407–2418. doi:10.1016/j.energy.2011.01.024.

[16] A. Dalla Rosa, H. Li, S. Svendsen, Modeling Transient Heat Transfer in Small-Size Twin Pipes for End-User Connections to Low- Energy District Heating Networks, Heat Transf. Eng. ISSN. 34 (2013) 372–384. doi:10.1080/01457632.2013.717048.

[17] L. Giraud, R. Baviere, M. Vallée, C. Paulus, Presentation, Validation and Application of the District Heating Modelica Library, Proc. 11th Model. Conf. (2015) 79–88. doi:10.3384/ecp1511879.

[18] B. Van Der Heijde, M. Fuchs, C.R. Tugores, G. Schweiger, K. Sartor, D. Basciotti, D. Müller, C. Nytsch-Geusen, M. Wetter, L. Helsen, Dynamic equation-based thermo-hydraulic pipe model for district heating and cooling systems, Energy Convers. Manag. 151 (2017) 158–169. doi:10.1016/j.enconman.2017.08.072.

[19] J. Dahm, District Heating Pipelines in the Ground - Simulation Model, 2001. http://trnsys.de/download/de/ts_type_313_de.pdf (accessed June 21, 2017).

[20] I. Gabrielaitiene, B. Bøhm, B. Sunden, Evaluation of Approaches for Modeling Temperature Wave Propagation in District Heating Pipelines, Heat Transf. Eng. 29 (2008) 45–56. doi:10.1080/01457630701677130.

[21] I. Gabrielaitiene, Numerical Simulation of a District Heating System with Emphases on Transient Temperature Behaviour, in: 8th Int. Conf. Environ. Eng., Vilnius, 2011: pp. 747–754. http://dspace.vgtu.lt/handle/1/1274.

ACCEPTED MANUSCRIPT

[22] I. Gabrielaitienė, B. Bøhm, B. Sundén, Dynamic temperature simulation in district heating systems in Denmark regarding pronounced transient behaviour, J. Civ. Eng. Manag. 17 (2011) 79–87. doi:10.3846/13923730.2011.553936.

[23] I. Gabrielaitiene, B. Sunden, B. Bøhm, H. Larsen, Dynamic performance of district heating system in Madumvej, Denmark, in: 10th Int. Symp. Dist. Heat. Cool., Hanover, 2006. http://www.lsta.lt/files/events/34_gabrielaitiene.pdf (accessed May 25, 2017).

[24] I. Gabrielaitiene, B. Bøhm, B. Sunden, Modelling temperature dynamics of a district heating system in Naestved, Denmark—A case study, Energy Convers. Manag. 48 (2007) 78–86. doi:10.1016/j.enconman.2006.05.011.

[25] I. Ben Hassine, U. Eicker, Control aspects of decentralized solar thermal integration into district heating networks, Energy Procedia. 48 (2014) 1055–1064. doi:10.1016/j.egypro.2014.02.120.

[26] F. Zanghirella, J. Canonaco, G. Puglisi, B. Di Pietra, Introducing solar thermal "net metering" in an actual small-scale district heating system: a case-study analysis, Energy Procedia. 101 (2016) 240–248. doi:10.1016/j.egypro.2016.11.031.

[27] M. Rämä, S. Mohammadi, Comparison of distributed and centralised integration of solar heat in a district heating system, Energy. 137 (2017) 649–660. doi:10.1016/j.energy.2017.03.115.

[28] C. Winterscheid, J.O. Dalenbäck, S. Holler, Integration of solar thermal systems in existing district heating systems, Energy. 137 (2017) 579–585. doi:10.1016/j.energy.2017.04.159.

[29] F.E. Toro, Riemann Solvers and Numerical Methods for Fluid Dynamics, Springer, Berlin, Heidelberg, 1999.

[30] T.L. Bergman, A.S. Lavine, F.P. Incropera, D.P. DeWitt, Fundamentals of Heat and Mass Transfer, 7th Editio, Wiley, 2011. https://books.google.it/books?id=vvyIoXEywMoC.

[31] P.D. Lax, Hyperbolic Systems of Conservation Laws and the Mathematical Theory of Shock Waves, Society for Industrial and Applied Mathematics, 1973. doi:doi:10.1137/1.9781611970562.ch1.

[32] G. Nellis, S. Klein, Heat Transfer, Cambridge University Press, Cambridge, MA, 2009.

[33] J.H. Lienhard, IV, J.H. Lienhard, V, A Heat Tranfer Textbook, Fourth Ed., Phlogiston Press, Cambridge, MA, 2017. http://ahtt.mit.edu.

[34] W.M. Kays, Convective Heat and Mass Transfer, McGraw-Hill, New York, NY, 1980.

ACCEPTED MANUSCRIPT

[35] K. Sartor, P. Dewalef, Experimental validation of heat transport modelling in district heating networks, Energy. 137 (2017) 961–968. doi:10.1016/j.energy.2017.02.161.

[36] K. Ciuprinskas, B. Narbutis, An Experimental investigation of Heat Losses in the District Heating Network, Energetika. 2 (1999) 35–40.

[37] H. Schlichting, K. Gersten, Boundary Layer Theory, 8th ed., Springer-Verlag, Berlin Heidelberg, 2000. doi:10.1007/978-3-662-52919-5.

ACCEPTED MANUSCRIPT